NON-STATIONARY RESPONSE ANALYSIS OF A HIGH-RISE BUILDING IN HAIKOU DURING TYPHOONS

Jiaxing HU[1*], Zhengnong LI[2], Zhefei ZHAO[3]

[1]School of Civil and Environmental Engineering, Hunan University of Science and Engineering,
Yongzhou, Hunan 425199, China
[2]Key Laboratory of Building Safety and Energy Efficiency of the Ministry of Education,
Hunan University, Changsha, Hunan 410082, China
[3]School of Vocational Engineering, Health and Sciences, RMIT University, GPO Box 2476,
Melbourne VIC 3001, Australia

Abstract. From 2014 to 2016, several wind resistant field measurements were conducted to the high-rise building in Haikou. Based on these measurements, the present paper disclosed the characteristics of the time-history responses of axial acceleration on different floors during four typhoons, including the Rammasun, Kalmaegi, Mujigae and Sarika typhoons. The modal parameters of the measured building were identified by Morlet time-frequency wavelet transform methods, and the amplitude-dependent modal damping ratios and frequencies along translational directions were investigated. The results show that the variation trend of modal frequency with acceleration amplitude identified by the Morlet wavelet is the same as that recognized by time-domain method, while it is scattered with the interval bar (min-average-max) due to the non-stationary response of typhoon. Meanwhile, the larger the amplitude of acceleration response of high-rise buildings under strong wind, the greater the time-varying fluctuation of modal parameters identified by wavelet transform, and the bigger the difference between the interval bar (min-average-max). The full-scale study is expected to provide useful information on the wind-resistant design of high-rise buildings in typhoon-prone regions.

Keywords: typhoon, high-rise building, non-stationary response, field measurement, Morlet.

Introduction

Modal parameters of high-rise buildings are extremely sensitive under strong winds due to the unique attributes of light weight, high flexibility and low damping in high-rise buildings. Thus, the modal parameters of high-rise buildings are widely identified by testing vibration signals of different floors on the basis of the natural frequency, damping ratio and mode-shapes. However, there are the obvious coupling effects between high-rise buildings and typhoons. The damping ratio mainly includes structural damping ratio and aerodynamic damping ratio, and the aerodynamic damping ratio are closely dependent on along-wind and across-wind fluctuating loads. And the fundamental frequency also changes with the increase of vibration amplitude.

Many related literatures have recorded the modal parameters of tall buildings with various geometric configurations under the boundary layer wind flows (Jeary, 1992; Tamura et al., 1995; Chen, 2013; Kwok & Melbourne, 1981; Kareem, 1982a, 1982b; Kwok, 1982; Kawai, 1992; Boggs, 1992; Vickery & Steckley, 1993; Piccardo & Solari, 1996; Isyumov, 1999; Tanaka et al., 2012). At present, the research results of modal frequency identification of high-rise buildings under typhoon action are relatively mature, but the research results of modal damping ratio identification of high-rise buildings are not very mature. Meanwhile, many investigators have studied the along-wind damping characteristics of high-rise buildings using wind tunnel tests. Marukawa et al. (1996) studied the wind-induced vibration responses and aerodynamic damping characteristics of rectangular cross sections with different width ratios and aspect ratios via adopting the double degree of freedom aeroelastic model. Cooper et al. (1997) applied forced vibration device to wind tunnel test, by which he studied the influence law of amplitude on along-wind

*Corresponding author. E-mail: *hjxcivil@163.com*

aerodynamic damping and compared the different results of along-wind aerodynamic damping calculated using wind tunnel test and quasi-steady method, respectively. The results demonstrated that the aerodynamic damping magnitude is independent of the amplitude of vibration. However, based on the wind tunnel test, Kareem (1978) claimed that the influences of aerodynamic damping on wind-induced vibration responses of high-rise buildings cannot be ignored. After that, the further researches of Kareem and Gurley (1996) and Vickery and Stekley (1993) showed that the influences of aeroelasticity effect; in particular, aerodynamic damping had to be considered when the reduced wind speed was more than 6.0 m/s to obtain more accurate wind vibration-induced responses. Gabbai and Simiu (2010) studied the aerodynamic damping on the along-wind response of tall building, and presented a novel methodology for the estimation of the aerodynamic damping that affects the along-wind response of tall buildings, the results of the calculations show that, the aerodynamic damping (1) is positive, that is, it has a favorable effect; (2) is small relative to the mechanical damping, it will thus be adopted in this paper to evaluate damping characteristics of the high-rise building during four typhoons, including the Rammasun, Kalmaegi, Mujigae and Sarika typhoons.

In summary, field measurements on the wind-induced response of high-rise buildings under typhoons are necessary to evaluate wind effect of high-rise buildings. Based on the non-stationary response of typhoon, this paper adopts Morlet-type time-frequency wavelet transform and presents different interval bar values (min-average-max) of modal frequency and damping ratio to study the time-frequency characteristics of modal parameter and to disclose the uncertain nature of natural frequency and damping ratio estimates. Besides, the first three modal frequencies under strong wind are identified by the Morlet wavelet.

1. Typhoon and instrumental information

No. 9 typhoon, rebadged as Rammasum, which was known as a super typhoon, landed in Wenchang city of Hainan province around 15:00 am on July 18, 2014. Rammasum has been regarded as the strongest typhoon which attacked China since 1949, the maximum wind grade reaches 17 near the typhoon centre during the passage of Rammasum, the minimum central pressure is 899 hPa, and the maximum wind velocity that affects Haikou city appears around 6:00 pm. No. 15 typhoon, designated as Kalmaegi, landed in Wenchang city of Hainan when landing province at 9:40 am on September 16, 2014. The wind velocity of Kalmaegi is 40.0 m/s when landing, the maximum wind grade reaches 13 and the central pressure is 960 hPa, the moving velocity is about 30 km/h, and the maximum wind velocity that affects Haikou appears around 11 am. No. 22 typhoon, named Mujigae, landed in Zhanjiang city of Guangdong province around 2:00 pm on October 4,

2015. The maximum wind grade reaches 15 (48.0 m/s) near the typhoon centre during the passage of Mujigae, the minimum central pressure of typhoon centre is 950 hPa, and the maximum wind velocity that affects Haikou appears around 11 am. No. 21 typhoon, called Sarika, landed in Wanning city of Hainan province at 9:50 am on October 18, 2016. The maximum wind grade reaches 14 (45.0 m/s) near the typhoon centre during the passage of Sarika, the minimum central pressure is 955 hPa, and the maximum wind velocity that affects Haikou appears around 10 am. The moving tracks and measuring point positions of typhoon Rammasun, Kalmaegi, Mujigae and Sarika are shown in Figure 1.

a) Typhoon Rammasum
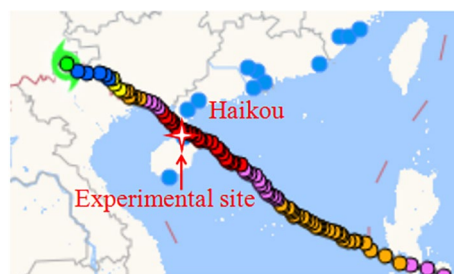
b) Typhoon Kalmaegi

c) Typhoon Mujigae

d) Typhoon Sarika

Figure 1. Moving tracks of typhoons Sarika, Mujigae, Kalmeagi, and Rammasun

The 32 story in situ building, whose viewing chamber locates at top floor, supported by 4 huge columns is the relatively higher building near this coastline. The height of its top floor is 108 m, aspect ratio is 6.71, and width-thickness ratio is 1.47. This in situ building locates on the north coast of Haikou, and is about 1.2 km from the coast. Although there are many buildings in the east of the in situ building, most of which are lower houses except for a few tall buildings (the heights of them are lower than 80 m). On the whole position, the in situ building locates in the northwest of the sea, thus having an open horizon. The data of wind speed, wind direction and acceleration were all collected by dynamic data acquisition system produced by Wuhan Yutek Electronic Technology Co., Ltd. The mechanical anemometer of RM.Young 05103V type was installed at a height of about 115 m to collect the wind field data. In order to examine the different floor acceleration responses near the wall corners, the acceleration data was gathered by the ultra-low frequency vibration gauge of 941 B type produced by Institute of Engineering Mechanics, CEA. Figure 2 provides the distributions of anemometer atop the building and acceleration pickup devices on the top floor.

2. Measured wind field and time histories of acceleration

2.1. Measured wind field atop the building

Employing the vector decomposition approach, the horizontal wind speed and direction were obtained by using the mechanical anemometer. The anemometer in the 0° direction was parallel to Y axis and its geographical direction was 11° north by west. The clockwise direction was designated as positive one. In another words, there were 90° from the anemometer in the 0° direction to X axis, as shown in Figure 2.

2.1.1. Measured wind filed data of Typhoon Rammasun

The recorded data within 23.8 h before and after the landing of Typhoon Rammasun at seaview Bay Building in Haikou at about 2:50 pm on July 17, 2014 were selected, and the inflow wind direction within the period of high wind speed was basically from 270° to 360°. Due to power outages in the process of measurement, only partial data during the period of high wind speed were recorded, and the maximum instantaneous speed reached 100.0 m/s. In the present paper, the basic time durations were defined as 10 min to measure mean wind speed and wind direction, and the measured maximum 10 min mean wind speed was 48.0 m/s. Figure 3 presents time history of partial wind field during the passage of Typhoon Rammasun.
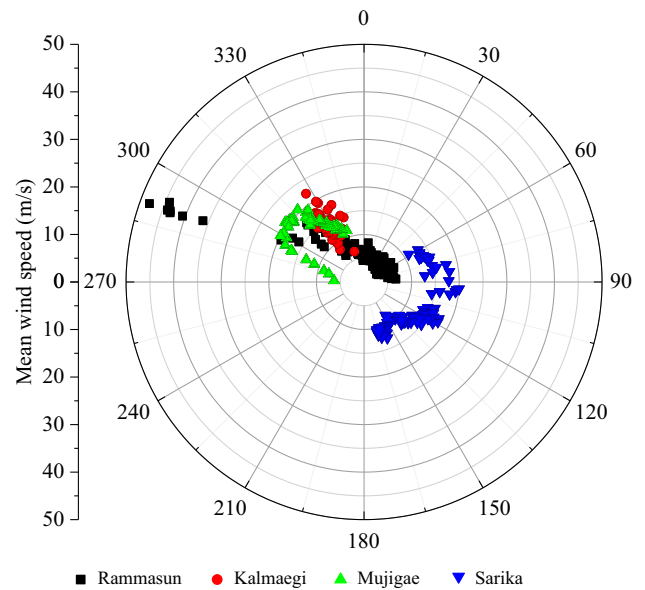
Figure 3. Wind field characteristics of Typhoons Sarika, Kalmaegi, Mujigae, and Rammasun

a) Building plan   b) A nemometer
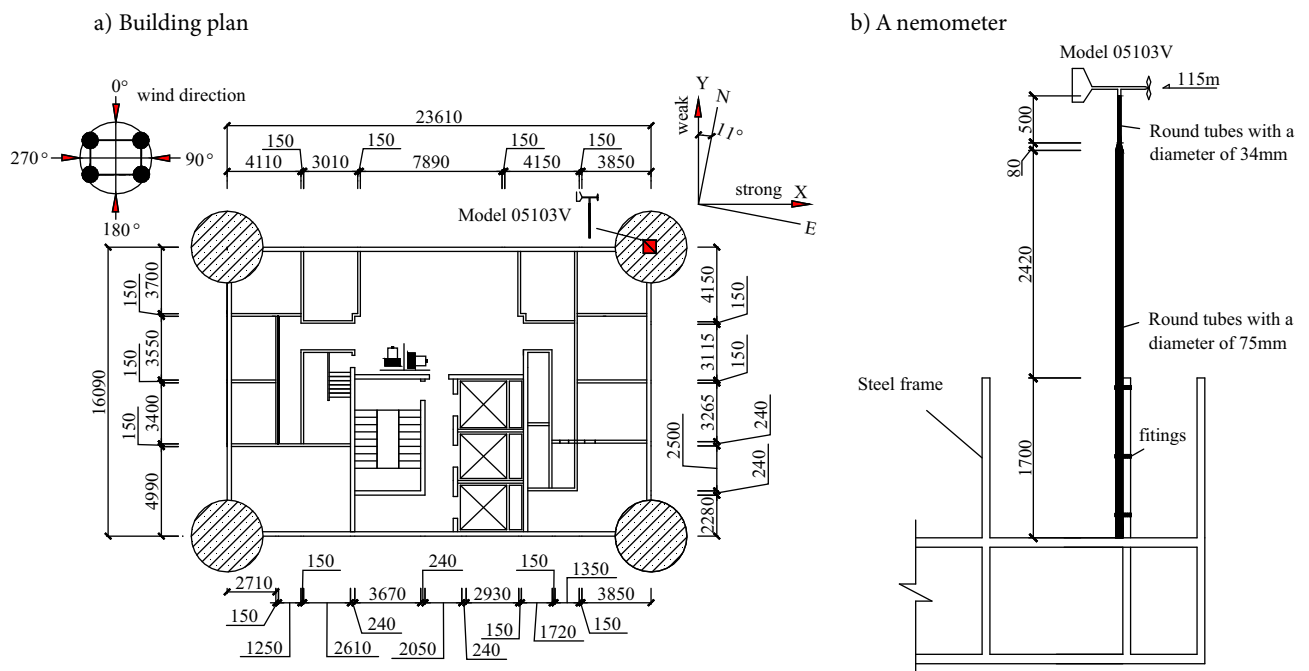
Figure 2. Distributions of anemometer atop the building and acceleration pickup devices on the top floor

2.1.2. Measured wind filed data of Typhoon Kalmaegi

The recorded data within 7.33 h before and after the landing of Typhoon Kalmaegi in Haikou at about 1:47 am on September 16, 2014 were selected. The maximum instantaneous speed was about 35.0 m/s, the inflow wind direction changed slightly from 310° to 350°, and high wind speed had a huge impact the in situ building in the Y-direction. It can be seen from Figure 3 that the measured maximum mean wind speed with the basic time duration of 10 min is about 22.3 m/s, the inflow wind direction is mainly within the range from 320° to 345°, and the mean wind direction just changes slightly as well.

2.1.3. Measured wind filed data of Typhoon Mujigae

The recorded data within 8.8 h after 4:28 am on October 4, 2015 were selected. The maximum wind speed was about 30.2 m/s and the inflow wind direction were mainly within the range from 250° to 360°. The measured maximum mean wind speed with the basic time duration of 10 min was about 20.4 m/s and the mean inflow wind direction was basically within the range from 270° to 345°. More details are shown in Figure 3.

2.1.4. Measured wind filed data of Typhoon Sarika

The recorded data within 18.3 h after 8:08 am on October 18, 2016 were selected. The maximum wind speed was

about 34.8 m/s and the inflow wind direction was basically within the range from 20° to 180°. The measured maximum mean wind speed was about 20.0 m/s when the basic time interval was defined as 10 min, and mean inflow wind direction was basically within the range from 0° to 180°. More details are shown in Figure 3.

2.2. Fluctuating wind power spectral density function

With the increasing in the height of the structure, the structure becomes more and more flexible and thus its vibration frequencies decrease. Due to the fact that the fluctuating wind speed energy centralizes in the regions of low frequency, the more flexible buildings are, the more obvious the wind-induced vibration effects are. The power spectral density (PSD) function of fluctuating wind speed was fitted out to examine the wind filed characteristics of these four typhoons, by which the concentrated frequency band of fluctuating wind energy was obtained and compared with Von Karmam spectrum. The measured fluctuation wind speed spectrum is shown in Figure 4 accompanying with Von Karmam spectrum.

As shown in Figure 4, the measured fluctuating wind speed spectrum for Typhoons Sarika, Mujigae, Kalmaegi, Rammasun agrees well with Karma spectrum. The fluctuating wind energy ranged from 0.1 Hz to 1.0 Hz, while
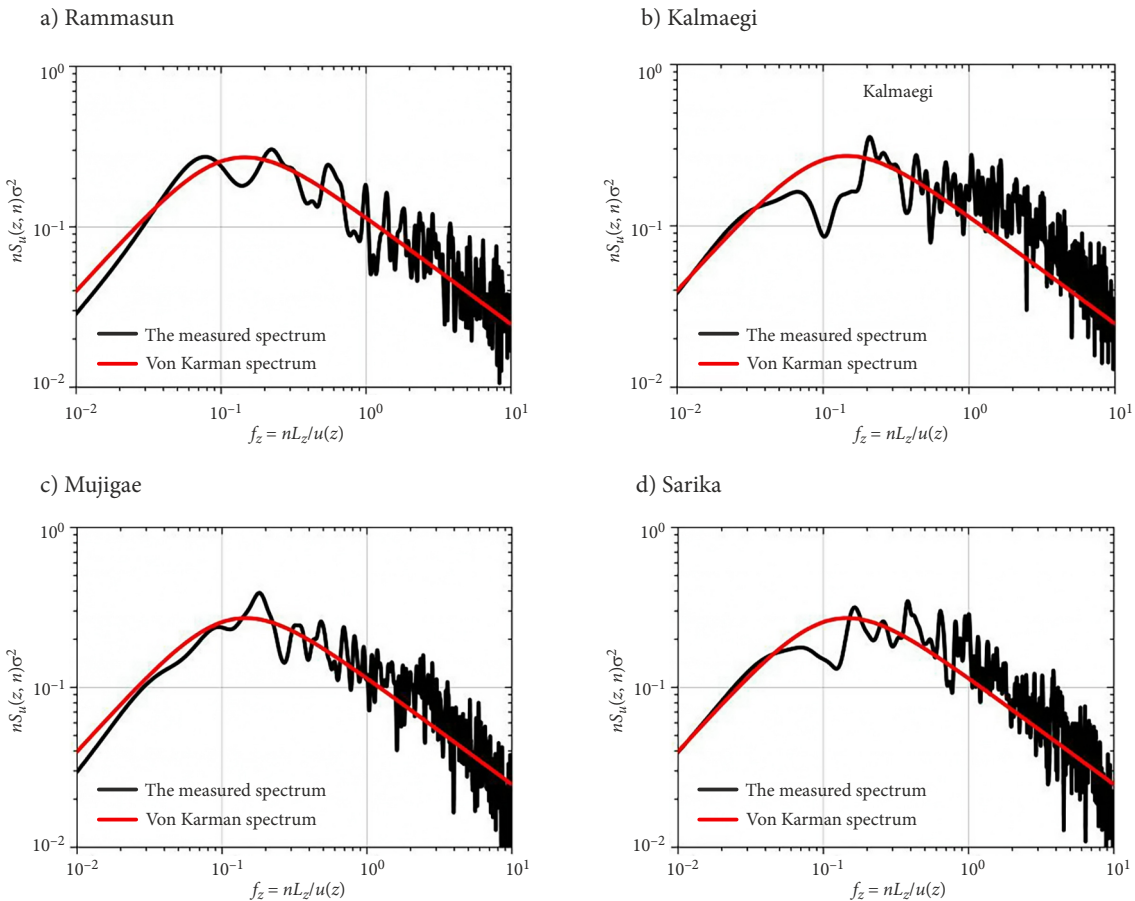
Figure 4. Measured fluctuation wind speed spectrum and Von Karmam spectrum on along-wind direction

the first-order vibration mode of measured building also located near this frequency band, leading to the coupling effects between the wind and building cannot be neglected (Thepmongkorn et al., 2002; Thepmongkorn & Kwok, 2002; Le & Caracoglia, 2015; Yong et al., 2011; Chen & Huang, 2009; Venanzi et al., 2014). Scrutinizing the aerodynamic effects in this frequency band thus was of great importance.

2.3. Measured time history of acceleration responses

The plane of the measured high-rise building is basically symmetrical. Each corner has a reinforced concrete cylinder with a diameter of 3 m. Each face is connected to four columns from the 3rd floor to the 30th floor by four diagonal cross trusses. The elevator shaft is located in the south of the middle, there is no refuge floor and structural reinforcement floor in the middle floor, and the mass and stiffness are distributed evenly along the height direction. Therefore, the coordinates of the rigid center and the center of mass of different floors are close, and the sensors are placed in the area near the rigid center and the center of mass of the structure (the area between the stairwell and the elevator shaft), which can effectively avoid the horizontal vibration measurement error caused by the torsional effect. Figure 5 presents the time history of acceleration responses at the 32nd floor along both X and Y axes in the passage of Typhoon Rammasun, and the peak values of acceleration along X and Y axes are 0.185 m/s^2 and 0.359 m/s^2, respectively. Figure 6 presents the time history of acceleration responses at the 32nd floor along both X and Y axes in the passage of Typhoon Mujigae and the peak values of acceleration responses along X and Y

axes are 0.033 m/s^2 and 0.044 m/s^2, respectively. The peak values of acceleration responses along X and Y axes at the 32nd floor under the influence of Typhoon Kalmaegi (Li et al., 2018) are 0.062 m/s^2 and 0.084 m/s^2, respectively. The peak values of acceleration responses along X and Y axes at the 32nd floor under the influences of Typhoon Sarika are 0.044 m/s^2 and 0.079 m/s^2, respectively (Hu et al., 2022). The stronger vibration appeared in the Y-axis direction.

In coastal areas, which are vulnerable to typhoon attacks, the occupants there will be disturbed when the acceleration responses brought about by typhoons are within the range from 0.150 m/s^2 to 0.500 m/s^2; and will feel uncomfortable within the range from 0.050 m/s^2 to 0.150 m/s^2 (Chang, 1973). Based on these indicators, under the influences of Typhoon Rammasun, the occupants felled uncomfortable; while under the influences of typhoons Kalmaegi, Mujigae, and Sarika residents had the feelings of disturbance.

3. Data preprocessing

3.1. Five-spot triple method

Due to the signal disturbances transmitted from power frequencies, double frequencies, and so on, there often existed obvious burrs in the measured data and large peak data in the time history curve of acceleration responses. These burrs presented as unsmooth peaks in the time history of measured data, if not removed immediately, they would have an impact on the mean values and variances of partial data. Therefore, five-spot triple method was used in this paper to carry out the interpolation substitution

a) X-axis　　　　　　　　　　　　　　　　　　　　　　　　b) Y-axis
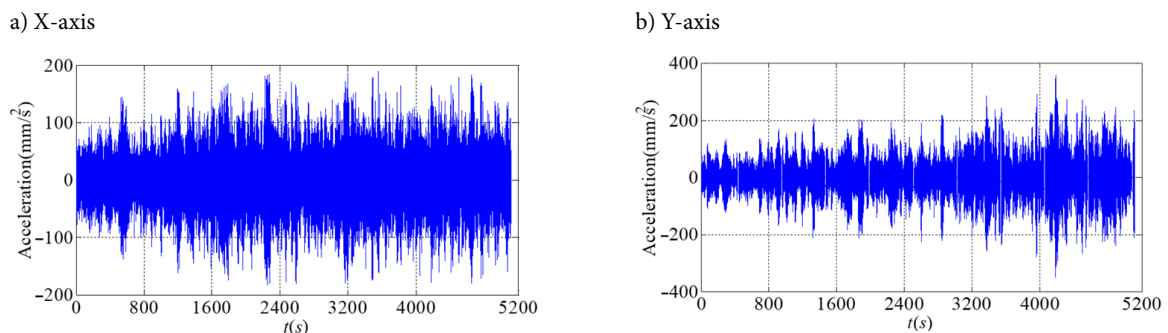
Figure 5. Time history of acceleration on the 32nd floor under the influences of Typhoon Rammasun

a) X-axis　　　　　　　　　　　　　　　　　　　　　　　　b) Y-axis
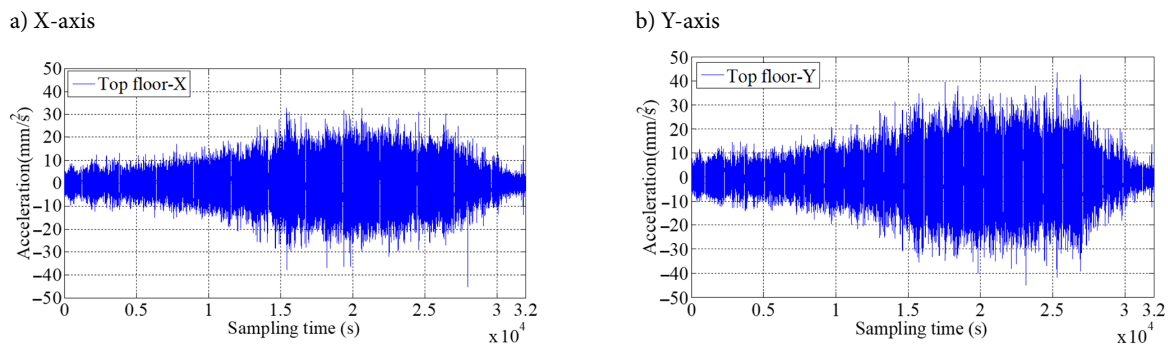
Figure 6. Time history of acceleration on the top floor under the influences of Typhoon Mujigae

with the aim of decreasing the deviations caused by burrs. The calculation formula of five-spot triple method can be expressed as follows:

$$\left.\begin{array}{l} y_1 = 1/70\left[69x_1 + 4(x_2 + x_4) - 6x_3 - x_5\right] \\ y_2 = 1/35\left[2(x_1 + x_5) + 27x_2 + 12x_3 - 8x_4\right] \\ \cdots\cdots\cdots\cdots\cdots\cdots\cdots\cdots \\ y_i = 1/35\left[-3(x_{i-2} + x_{i+2}) + 12(x_{i-1} + x_{i+1}) + 17x_i\right] \\ \cdots\cdots\cdots\cdots\cdots\cdots\cdots\cdots \\ y_{m-1} = 1/35\left[2(x_{m-4} + x_m) - 8x_{m-3} + 12x_{m-2} + 27x_{m-1}\right] \\ y_m = 1/70\left[-x_{m-4} + 4(x_{m-3} + x_{m-1}) - 6x_{m-2} + 69x_m\right] \end{array}\right\} (i = 3, 4, \cdots, m-2),$$

$$(1)$$

where $y_1, y_2, y_i, y_{m-1}, y_m$ are, respectively, the corresponding data of $x_1, x_2, x_i, x_{m-1}, x_m$ after being processed by using five-spot triple method.

3.2. Removing trend item of polynomial

Due to such factors as zero fluctuation of amplifier caused by the temperature variations, the unstable low-frequency of sensors beyond frequency range, as well as the environment disturbance around sensors, the data of vibration signal collected in vibration measurement will deviate from baseline, and the deviation value will change as time evolved. The trend items of signals refer to the whole process of deviation baseline that changes as time passes. Likewise, the least square method is adopted in this paper to remove this trend item of polynomial. Employing $\{x_k\}(k = 1, 2, 3, \cdots, n)$ and $\{\overline{x_k}\}$ to represent the sample data and the trend item of polynomial function of measured vibration signals, respectively, the calculation formula of removing trend item of polynomial can then be written as

$$y_k = x_k - \overline{x_k} \quad (k = 1, 2, 3, \cdots, n). \qquad (2)$$

3.3. Bandwidth digital filtering

To obtain independent acceleration responses of high-rise buildings along both X and Y axes, instead of the acceleration response data along X and Y axes mutually disturbed under the influences of typhoons, the band-pass filtering was applied to process the measured data of acceleration responses. Employing the frequency methodology of digital filtering, the data of input signals was processed using FFT to analyze the frequency spectrum of acceleration responses. The formula of frequency analysis method for the digital filtering is given by

$$y(r) = \sum_{k=0}^{N-1} H(k) X(k) \exp(j2\pi kr/N), \qquad (3)$$

where X is the discrete Fourier transformation to input signal x; H is the frequency responses of filter. Because the first-order natural vibration frequencies of the structure in the X and Y axes are about 0.67 Hz and 0.57 Hz, respectively, the pass-band range of filter along the X and Y axes was set as $f \in (f_i - 0.08f_i, f_i + 0.08f_i)$. Hence, the pass-band range of filter was 0.62 Hz~0.72 Hz along the X axis, while 0.52 Hz~0.62 Hz along the Y axis.

Intercepting the 10 min duration in the measured acceleration data and employing both the five-spot triple and least square methods to remove polynomial trend item as well as bandwidth digital filtering, the acceleration time history then is obtained under different treatment processes. Subsequently, by resorting to the RDT (Jeary, 1992; Li et al., 2018), the free damping curve was attained when the benchmark interception amplitude was 1.5 times standard deviation. It is seen from Figure 7 that the curve of measured data is smooth and appears well-organized damping after being processed by band-pass filtering.
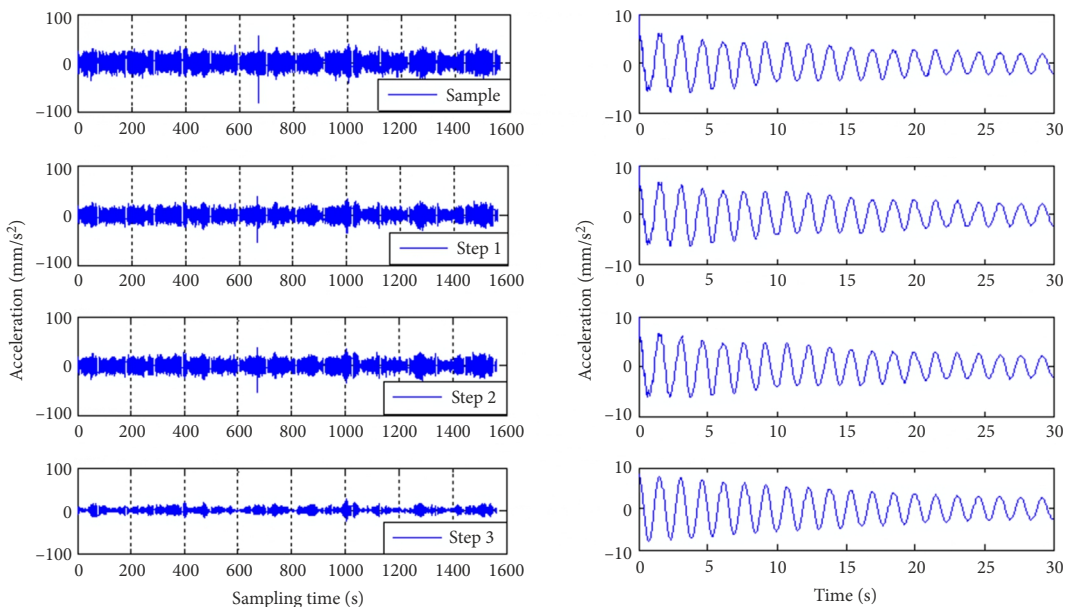
Figure 7. Comparisons of random decrement signatures after being processed by RDT: Step 1 – the data after being processed by five-spot triple method; Step 2 – the data after being removed from multinomial trend items on the basis of Step 1; Step 3 – the data after being processed by band pass filtering on the basis of Step 2

By writing MATLAB program to conduct Fourier transform, the measured power spectrum intensity at each floor of the building was obtained. The auto-power spectral density function is given by:

$$S_{pp}(\omega_i) = \frac{1}{MN_{FFT}} \sum_{j=1}^{M} X_{pj}(\omega_i) X^*_{pj(\omega_i)}, \qquad (4)$$

where $X_{pj}(\omega_i)$ denotes the Fourier transform of random vibration acceleration responses of a measuring point at the jth data segment, $X^*_{pj(\omega_i)}$ is the conjugate complex of $X_{pj}(\omega_i)$, N_{FFT} represents the data length of Fourier transform, and M is the average times. Figure 8 shows the measured power spectral density functions along both the X and Y axes.

It can be seen from Figure 8 that the wind-reduced responses at the first mode of the high-rise building along the X and Y directions accounted for the majority in the total response. Judging from the curve of fluctuating wind power spectrum density, the fluctuating wind energy concentrated in the low frequency stage and approached the fundamental natural frequency of the high-rise building. The first-order natural vibration frequency along the X axis was about 0.67 Hz, while the frequencies identified by the RDT mostly ranged from 0.64 to 0.70 Hz under different mean wind speeds. The first-order natural vibration frequency along the Y axis was about 0.57 Hz, while the frequencies identified by the RDT mostly ranged from 0.55 Hz to 0.59 Hz under different mean wind speeds.

a) Auto-power spectral density along X axis
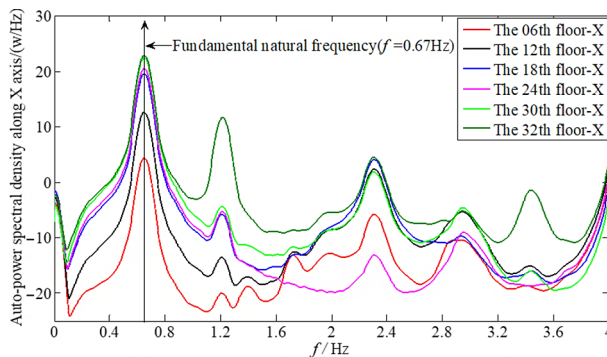
b) Auto-power spectral density along Y axis
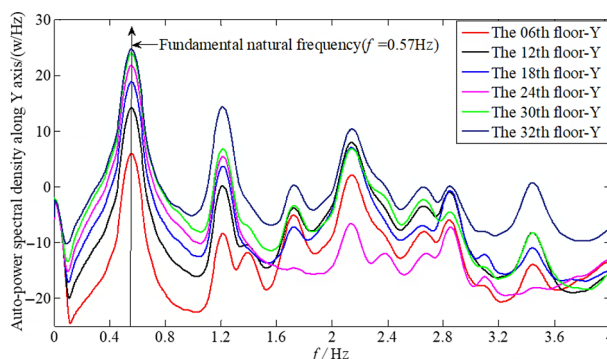
Figure 8. Measured power spectral density functions along both the X and Y axes

Because the first-order natural vibration frequencies identified by the auto-power spectral density function were in the ranges of those identified by the RDT, thus proving that there is high accuracy in processing measured data using RDT.

4. Modal parameter identifications

The recently developed wavelet analysis technology is a time-scale analysis method (time-frequency) of signals. With the characteristics of multi-resolution analysis, it can represent the local characteristics of signals in both time and frequency domains. Therefore, it is a time-frequency localization analysis method that can change both time and frequency windows. Wavelet transform, which utilizes both time and frequency domain information of signals, is an essential focus for developing modal parameter identification technology. Based on the previous studies and the basic principle of the NExT method, the paper uses cross-correlation function as the free-response data of the system and adopts the non-orthogonal continuous Morlet wavelet as the mother wavelet. Also, the critical technologies of modal parameter identification, including modal identification under environmental excitation, are further discussed.

4.1. Morlet-type time-frequency wavelet transform

In this paper, a non-orthogonal continuous complex Morlet wavelet used as a mother wavelet. The reasons are as follows: (1) The amplitudes of real and imaginary parts of complex Morlet wavelet are exponentially attenuated simple harmonic vibration signals, which are consistent with the free-response signals of dynamic systems; (2) Binary orthogonal wavelet can reconstruct signals well, but its scale discredited in binary. Therefore, the frequency resolution of the wavelet transform will constrain due to its discretization. However, the continuous wavelet transforming of the signal using non-orthogonal Morlet wavelet without scale function can realize arbitrary high resolution in a time domain and frequency domains. The advantage of complex Morlet wavelet can identify dense modes well. Morlet wavelet defined as:

$$\varphi(t) = e^{j\omega_0 t} e^{-t^2/2}; \qquad (5)$$

$$\Phi(\omega) = \sqrt{2\pi} e^{-1/2(\omega-\omega_0)^2}. \qquad (6)$$

Eqns (5) and (6) show that the waveforms of Morlet wavelet in both time and frequency domains are in the form of Gauss window function. Thus modes at all orders can be separated easily. The free-response signal of the multi-degree-of-freedom viscous damped system is assumed as follows:

$$x(t) = \sum_{k=1}^{P} B_k e^{-k \ n_k t} \cos(\omega_{dk} t + \theta_{Ok}), \qquad (7)$$

where P is the order; $\Delta\varphi$ is the undamped natural frequency at the kth order; $\varphi''(x)^2 < \varphi'(x)^2$ is the damping ratio at the kth order; $\bar{k}_2^* = k_2^* - k_{G2}^* < \bar{k}_1^* = k_1^* - k_{G1}^*$ is the

damped frequency of the system at the *k*th order. Also, the conditions satisfy:

$$\omega_{dk} = \omega_{nk}\sqrt{1-\zeta_k{}^2}.\qquad(8)$$

The wavelet transform of Eqn (5) can be expressed as:

$$W(a,b) = \frac{\sqrt{a}}{2}\sum_{k=1}^{P}B_k e^{-\zeta_k\omega_{nk}b}\Phi^*(a_i\omega_{dk})e^{j(\omega_{dk}b+\theta_{0k})}.\qquad(9)$$

Based on the principle of convolution, the coefficients of wavelet transform reflect the similarity between the wavelet function and the signal to be identified. Therefore, only when $a\omega_d = \omega_0$ and $a = a_i = \omega_0/\omega_{dk}$, $|W(a, b)|$ can achieve the maximum value for the fixed *a*:

$$\left|W(a_i,b)\right| = \frac{\sqrt{a_i}}{2}Be^{-\zeta\omega_n b}\left|\Phi^*(a_0\omega_d)\right|.\qquad(10)$$

The logarithm of both sides in Eqn (7) is:

$$\ln\left|W(a_i,b)\right| = -\zeta\omega_n b + \ln(\frac{\sqrt{a_0}}{2}B\left|\Phi^*(a_0\omega_d)\right|).\qquad(11)$$

The phase of wavelet coefficients is:

$$\angle W(a_0,b) = \omega_d b + \varphi_o.\qquad(12)$$

Eqns (11) and (12) are univariate functions of *b*. The slopes assumed as k_1 and k_2, that is, $k_1 = -\zeta\omega_n$ and $k_2 = \omega_d$, respectively. After combining Eqn (8), the undamped natural frequencies and damping ratios at the *i*th order are:

$$f_i = \frac{\sqrt{k_1^2+k_2^2}}{2\pi};\qquad(13)$$

$$\zeta_i = -k_1/2\pi f_i.\qquad(14)$$

The wavelet transform coefficient $W(a, b)$ is involved, which contains both amplitude and phase information. In this paper, the wavelet transform coefficients of each measuring point are used to identify each order mode of the system. The response point of the system assumed as *j*; The reference point is *r*; the corresponding wavelet transform coefficients of the *i* order are $W^j(a_i, b)$ and $W^r(a_i, b)$, and the ratio between them is:

$$\Phi_i^j = W^j(a_i,b)/W^r(a_i,b).\qquad(15)$$

Eqn (15) reflects the vibration information of response point *j* relative to the reference point *r*. In the actual calculation, the ratio of time-variable *b* in Eqn (10) is not a constant. Therefore, the optimum consistent solution should be obtained for the normalized coefficient of each mode shape ϕ_i^j of each response point that is relative to each reference point. The least square method is adopted to realize the optimum constant solution. In Eqn (15):

$$W_j = W^j(a_i,b);\qquad(16)$$

$$W_r = W^r(a_{ib},b).\qquad(17)$$

The least square solution of ϕ_i^j is:

$$\phi_i^j = \left(W_r^H W_r\right)^{-1}W_r^H W_j,\qquad(18)$$

where W_r^H is the Conjugate transpose function of W_r.

4.2. Modal parameter identification results

Figure 9 shows the measured acceleration response data of five stories along Y-axis. Figure 10 illustrates the results of the two-dimensional and three-dimensional time-frequency domain analysis by Morlet-type time-frequency wavelet transform, indicating that the first three time-frequency domain characteristics exert great interference in acceleration signal recognition. To improve the recognition accuracy of the Morlet wavelet method, the measured time history data of acceleration response firstly decomposed in reference to the first three order vibration signals of high-rise buildings. The frequency-domain decomposition bandwidths are 0–1 Hz, 1.5–3 Hz and 3.5–5 Hz, respectively. Then 5 column raw response data of the first three order vibration signals obtained, from which the cross-correlation function matrices of the array with the size of 5×5 obtained. After that, five cross-correlation function curves of $R_{6\&6}$, $R_{6\&12}$, $R_{6\&18}$, $R_{6\&24}$ and $R_{6\&30}$ of the first three orders are also obtained. Figure 11 presents the decomposition signals results of the cross-correlation function at the first three orders along Y-axis. Five correlation function signals at the first three orders are processed
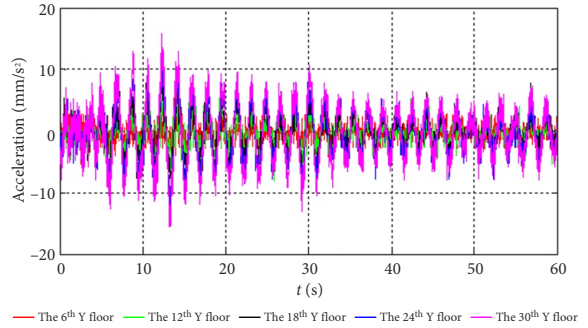
Figure 9. The measured acceleration response data of five storeys along Y-axis

a) Wavelet time-frequency plane diagram
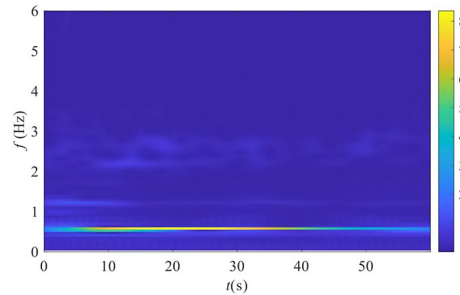
b) Wavelet time-frequency three-dimensional diagram
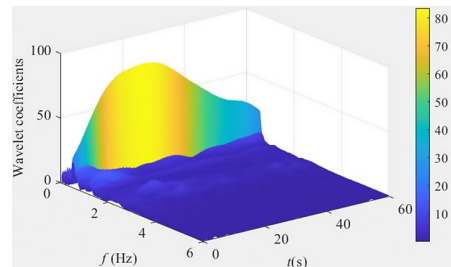
Figure 10. Analysis results of wavelet time-frequency domain

by wavelet transform, by which the wavelet time-frequency graph and the fitting chart between the amplitude and phase of wavelet transform coefficients are attained. Finally, the modal frequency, damping ratio and mode shape of the high-rise building are identified.

The cross-correlation function of $R_{6\&30}$ within the bandwidth 0~1 Hz along Y-axis is firstly taken as an example in this paper, and the wavelet time-frequency graph through the wavelet transform is obtained, and the modal frequency at the first order is 0.576 Hz, as shown in Figure 12. Figures 13a and 13b show the fitting curves of the amplitude and phase of the corresponding wavelet transform coefficients. Based on the above methods and cross-correlation function, the first three mode shapes, frequencies and damping ratios of the high-rise building are identified, as shown in Figure 14.

a) The 1st mode decomposed results: cross-correlation

b) The 2nd mode decomposed results: cross-correlation

c) The 3rd mode decomposed results: cross-correlation
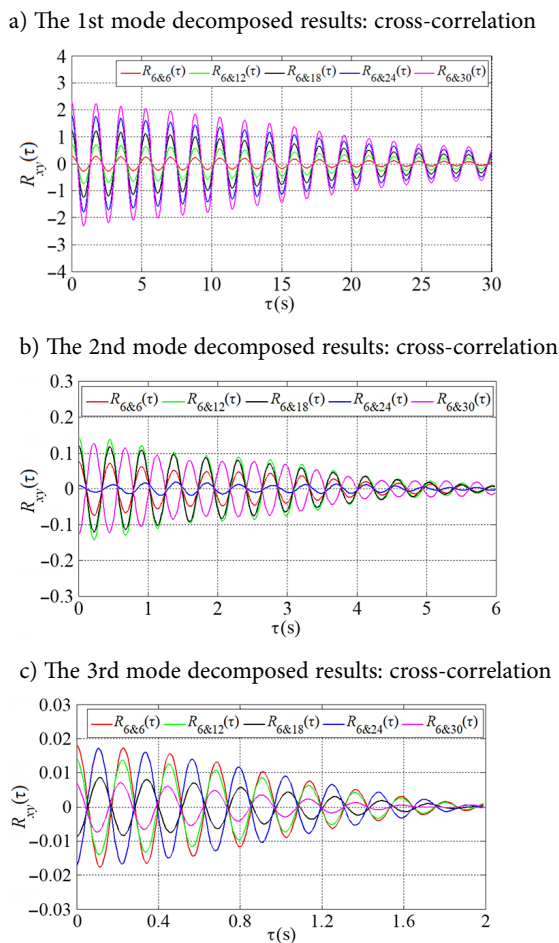
Figure 11. Cross-correlation functions on different floors along Y-axis
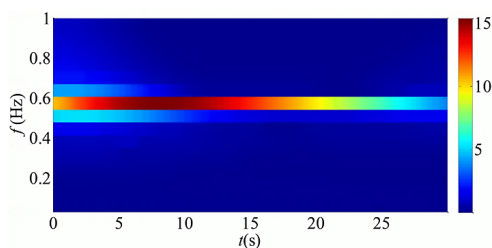
Figure 12. Wavelet time-frequency diagram

5. Amplitude-dependent modal parameters

5.1. Sample selection

Dynamic response measurement includes various physical parameters such as displacement, velocity and acceleration, but it is difficult to measure those parameters in that the displacement and the velocity of different floors are strictly related to the ground, and the vibration balance centre and initial displacement as well as velocity of the measured building are always changing. Therefore, acceleration responses of different floors are recorded to identify the amplitude-dependent modal parameters. The relationship between acceleration amplitude and modal parameters is widely analyzed to investigate the non-linear characteristic of high-rise buildings in strong wind condition.

As defined in the Chinese National Loading Specification for Building Structures (GB 5009-2012) (The Ministry of Housing and Urban-Rural Development, 2012), the basic wind pressure is the maximum wind speed recorded by local meteorological stations over the years. According to the basic wind speed, the annual maximum wind speed of different anemometer heights and time intervals is converted to the 10-min annual maximum wind speed on average that is recorded at the height of 10 m from the ground. The maximum wind speed in 50 years appears during the return period and is determined as the local basic wind speed. The basic wind pressures during the return period for 10, 50 and 100 years in Haikou City are 0.45 kN/m², 0.75 kN/m² and 0.90 kN/m², respectively.

a) Fitting amplitude of wavelet transform coefficient

b) Fitting phase of wavelet transform coefficient
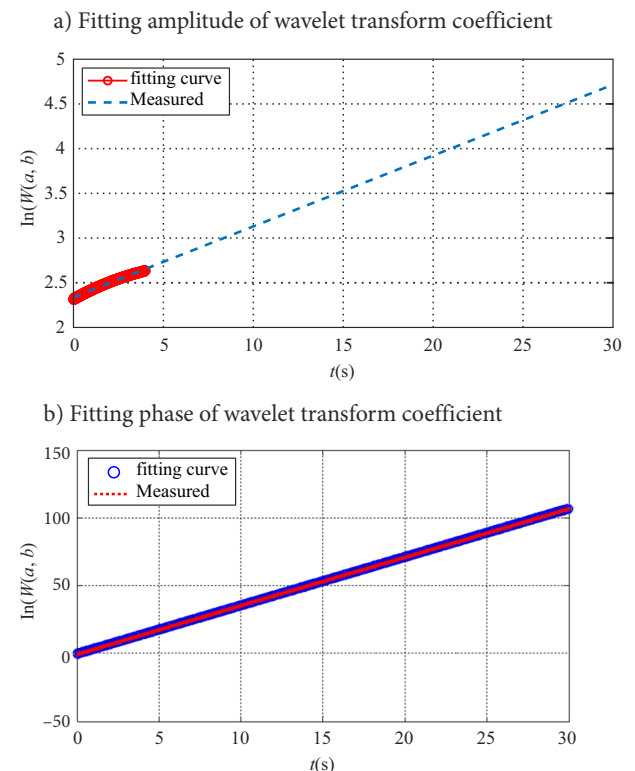
Figure 13. Fitting amplitude and phase of wavelet transform coefficient using R6&30

a) X – 1st-mode

f_{1st} = 0.650 Hz

ζ_{1st} = 2.09%

b) X – 2nd-mode

f_{2nd} = 2.33 Hz

ζ_{2nd} = 1.97%

c) X – 3rd-mode

f_{3rd} = 4.163 Hz

ζ_{3rd} = 2.39%

d) Y – 1st-mode

f_{1st} = 0.576 Hz

ζ_{1st} = 2.66%

e) Y – 2nd-mode

f_{2nd} = 2.176 Hz

ζ_{2nd} = 1.59%

f) Y – 3rd-mode

f_{3rd} = 4.352 Hz

ζ_{3rd} = 1.47%
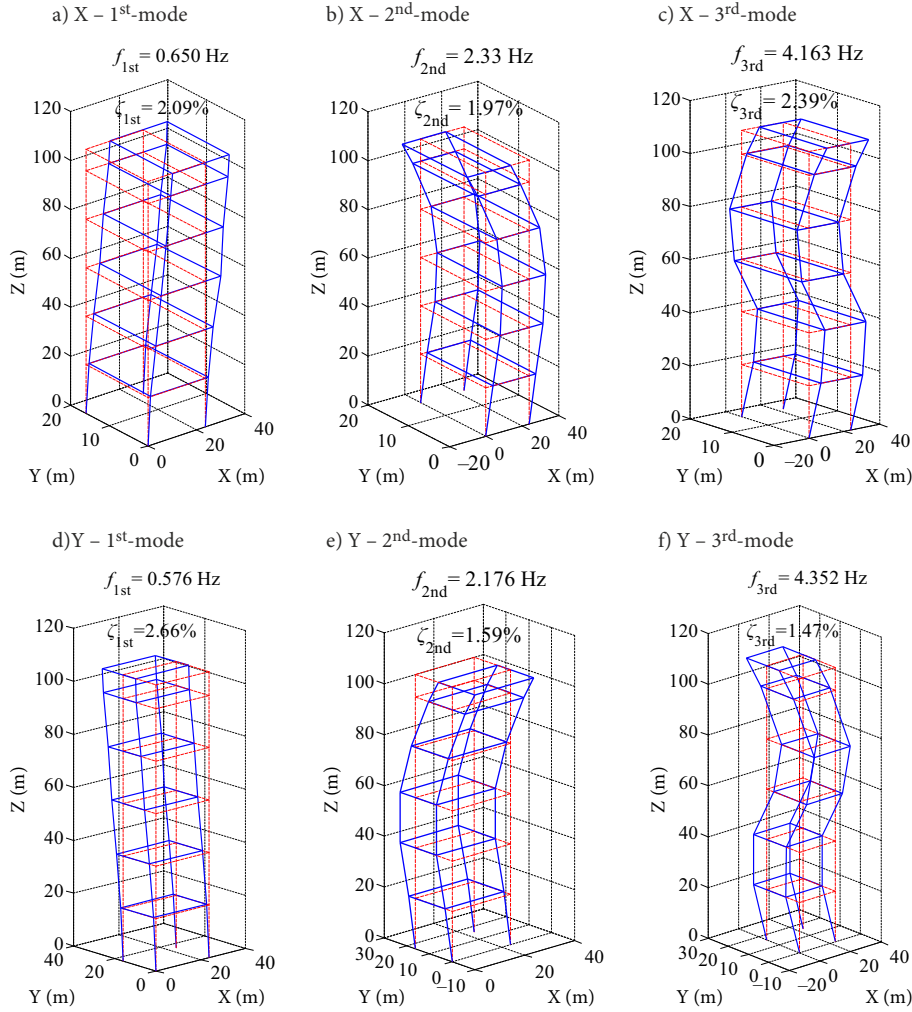
Figure 14. The first three modal parameters under ambient excitations identified by Morlet-type time-frequency wavelet transform

Therefore, a 10-min time interval is selected for analyses in this paper to compare the related parameters with those in the Chinese load code. When studying the characteristics of modal parameters under typhoon excitation, the wind direction of the 10-min sample changes constantly in the process of typhoon landing, thus the included angle between wind direction and vibration direction of X and Y axes should be strictly controlled to avoid excessive deviation. The wind direction under typhoon Sarika in high wind speed and the large amplitude of dynamic response are prone to the X-axis. This study set the wind direction close to X-axis as the along-wind vibration, and Y-axis as the cross-wind vibration. The absolute values of the included angles strictly controlled from 0° to 10°. It can be approximated that the along-wind load of typhoon mainly affects the X-axis vibration response, while the cross-wind load primarily affects the Y-axis vibration response.

It's necessary to study the modal damping ratio and frequency characteristics of high-rise buildings under large acceleration amplitudes. This paper adopts RDT and Morlet-type time-frequency wavelet transform methods to identify the amplitude-dependent modal frequency and damping ratio. As a favorable method to analyze the non-linear damping characteristics, RDT is widely used

to obtain accurate mode identification of non-stationary and non-linear responses. In order to obtain the first three modal parameters along X and Y axes, the measured signals of acceleration responses are processed by the reasonable band-pass filtering. Firstly, the ranges of band-pass filters along X and Y axes are determined as $f \in (f_i - 0.08 f_i, f_i + 0.08 f_i)$, f_i is the modal frequency identified by the APSDF with 10-min. After that, the modal frequency and damping ratio are obtained by fitting the peak values of the free vibration decay curve by RDT. Based on the measured dynamic response during Typhoon Sarika, the modal frequencies and damping ratios of the high-rise building under Typhoon Sarika are identified by RDT and Morlet-type time-frequency wavelet transform methods with an interval of 10-min.

5.2. The amplitude-dependent modal frequency

In this paper, the 10-min modal parameters are the average values of the measured modal parameters of the high-rise building within 10 minutes. The average values of modal parameters are used to calculate the dynamic characteristics, including wind vibration characteristics of high-rise buildings in the time interval of 10 minutes. If the basic

time interval is reduced or enlarged, modal parameters with different time intervals will fluctuate according to the average values of 10-min modal parameters due to the different RMS of Acc. However, modal parameters fluctuating with average values can only reflect the average values of modal parameters within the corresponding time intervals. More importantly, modal identification accuracy is closely related to the signal quality and signal length. If the analysis time interval is too small, the accuracy of modal parameter identification will reduce. On the variation of estimates of modal frequency and damping ratio since non-stationary response, therefore, this paper adopts Morlet-type time-frequency wavelet transform to study the time-frequency characteristics of modal parameter and understand the nature of uncertainties of the natural frequency and damping ratio estimates, presented with the interval bar (min-average-max) values of modal frequency and damping ratio. The first three modal frequencies under strong wind are identified by the Morlet wavelet, and the recognition results are presented in Figure 15. The variation trend of modal frequency with acceleration am-

plitude determined by the Morlet wavelet is the same as that recognized by time-domain method.

Considering the non-stationary response of typhoon, the measured modal frequencies and acceleration amplitudes are analyzed with a basic time interval of 1 minute. The first three modal frequencies under strong wind are identified by the Morlet wavelet, and the recognition results are presented in Figure 16. The variation trend of the 1-min modal frequency with acceleration amplitude determined by the Morlet wavelet is the same as that recognized by time-domain method. The modal frequency is relatively stable when the basic time interval is 10 minutes, while it is scattered when the basic time interval is 1 minute. The phenomenon reveals that the larger the analysis time interval is, the more stable the analysis results are.

5.3. The amplitude-dependent damping ratio

The damping ratios of the measured high-rise building include structural damping ratio and aerodynamic damping ratio during Typhoon Sarika. Figure 17 shows the ranges of the measured damping ratio at the first three modes
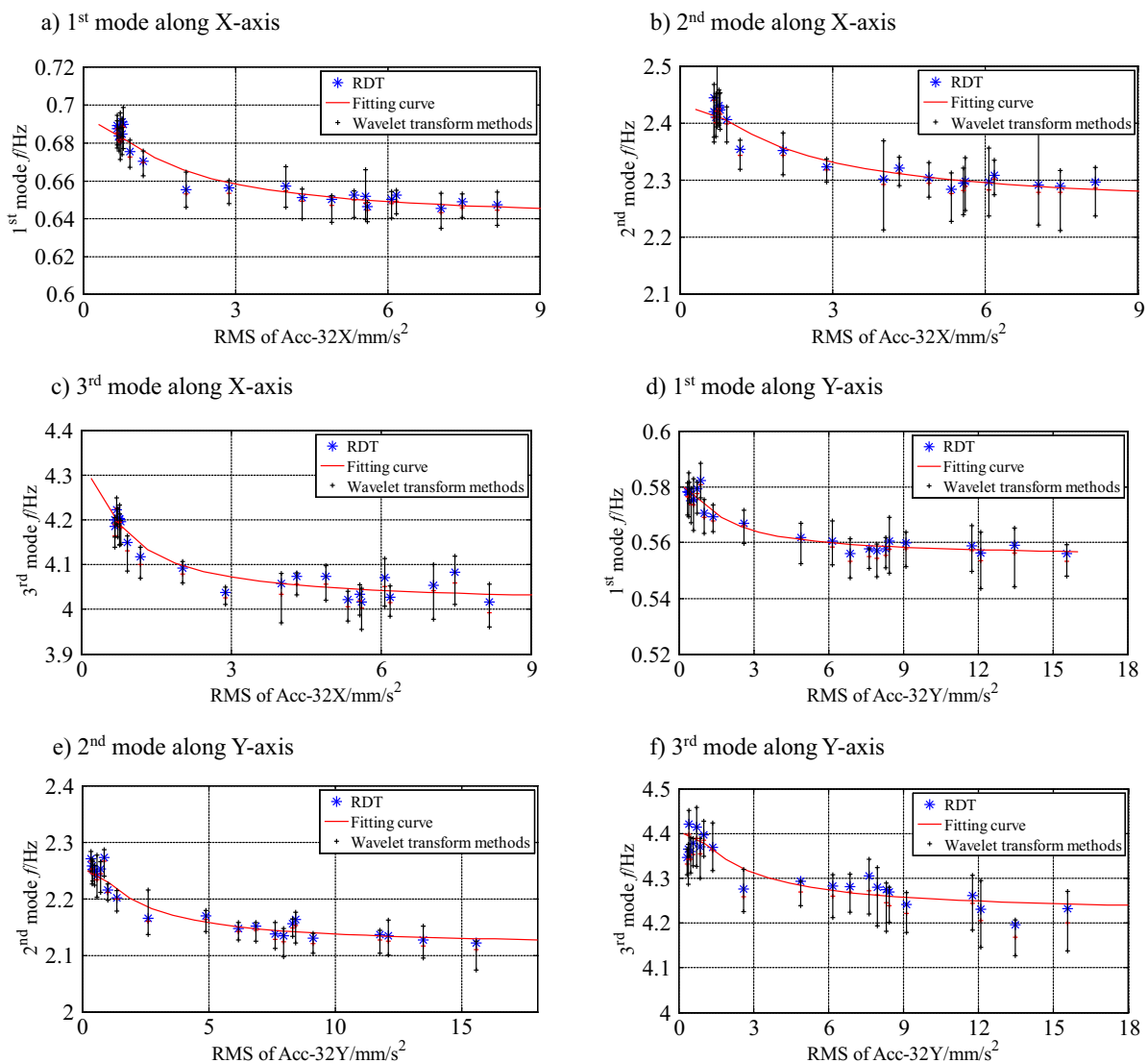
Figure 15. The relationship between modal frequency and RMS of Acc at the top floor

a) 1st mode along X-axis

b) 2nd mode along X-axis

c) 3rd mode along X-axis

d) 1st mode along Y-axis

e) 2nd mode along Y-axis

f) 3rd mode along Y-axis
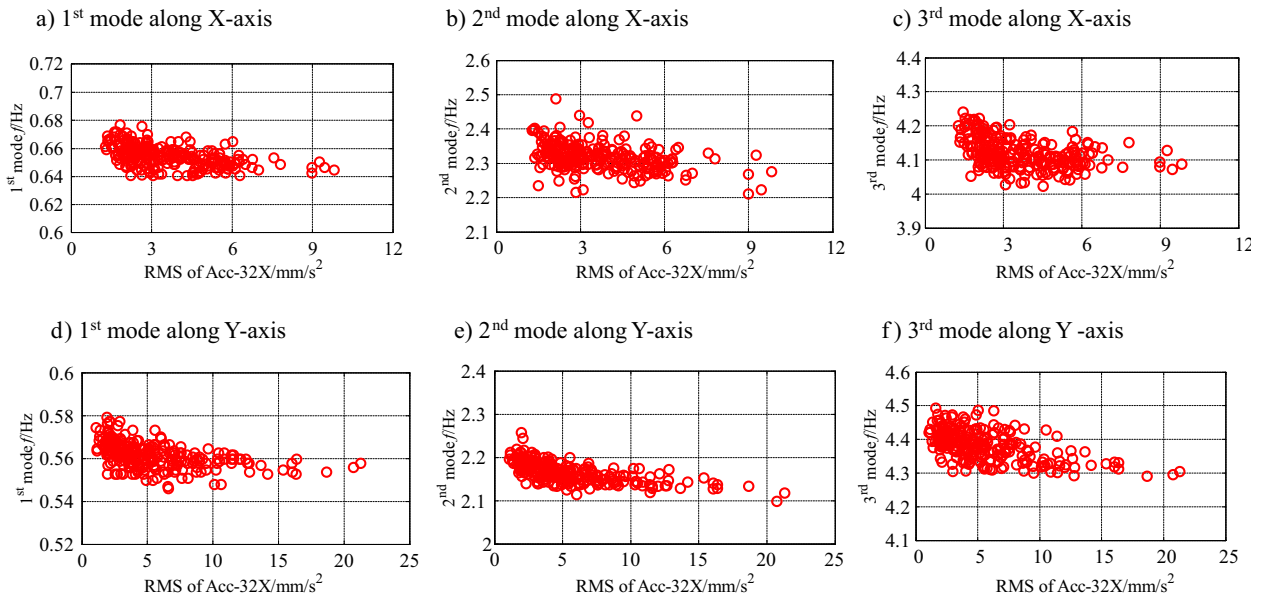
Figure 16. The relationship between modal frequency and RMS of Acc at the top floor

a) 1st mode along X-axis

b) 2nd mode along X-axis

c) 3rd mode along X-axis

d) 1st mode along Y-axis

e) 2nd mode along Y-axis

f) 3rd mode along Y-axis
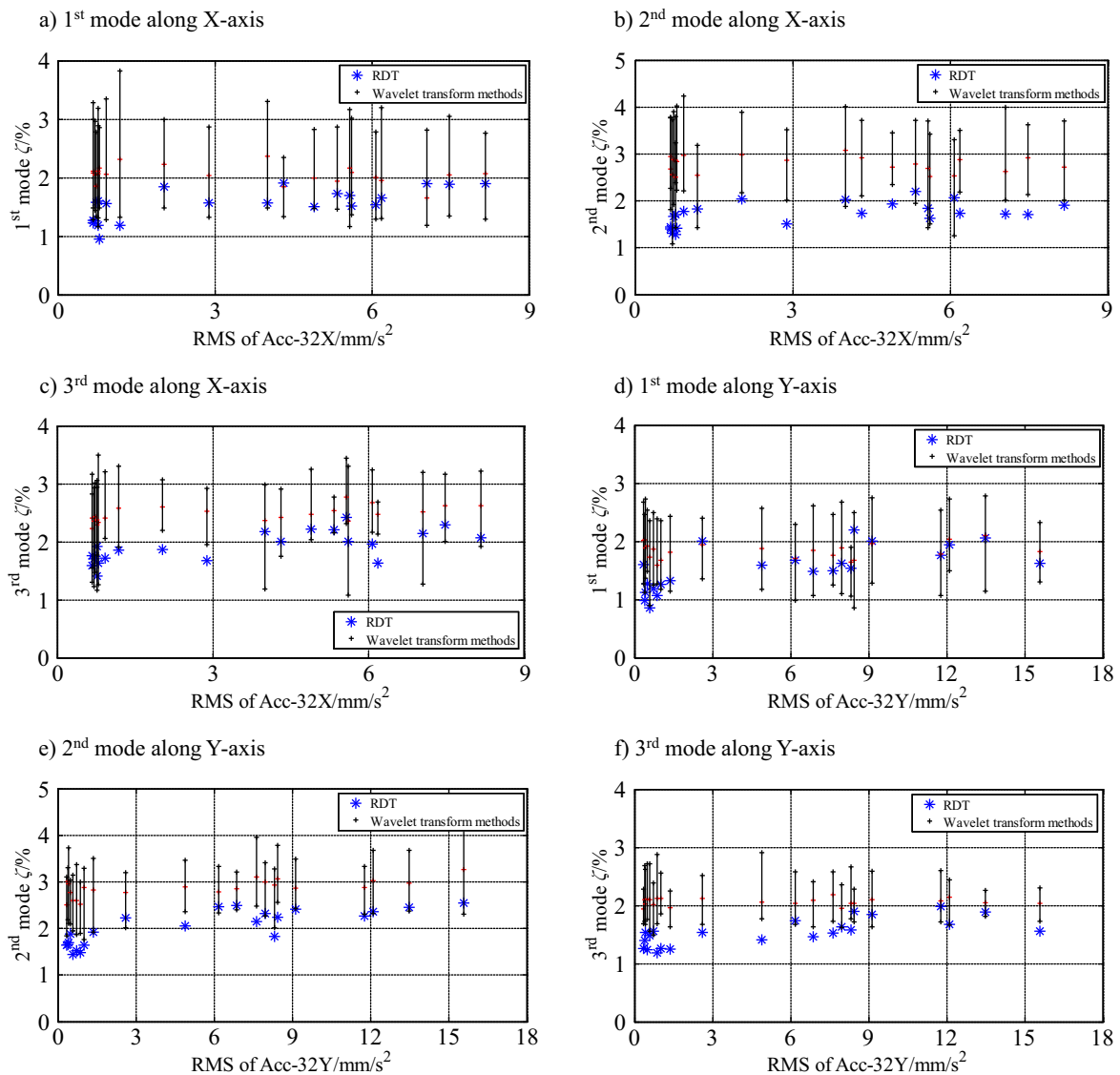
Figure 17. The relationship between modal damping ratios and RMS of Acc at the top floor
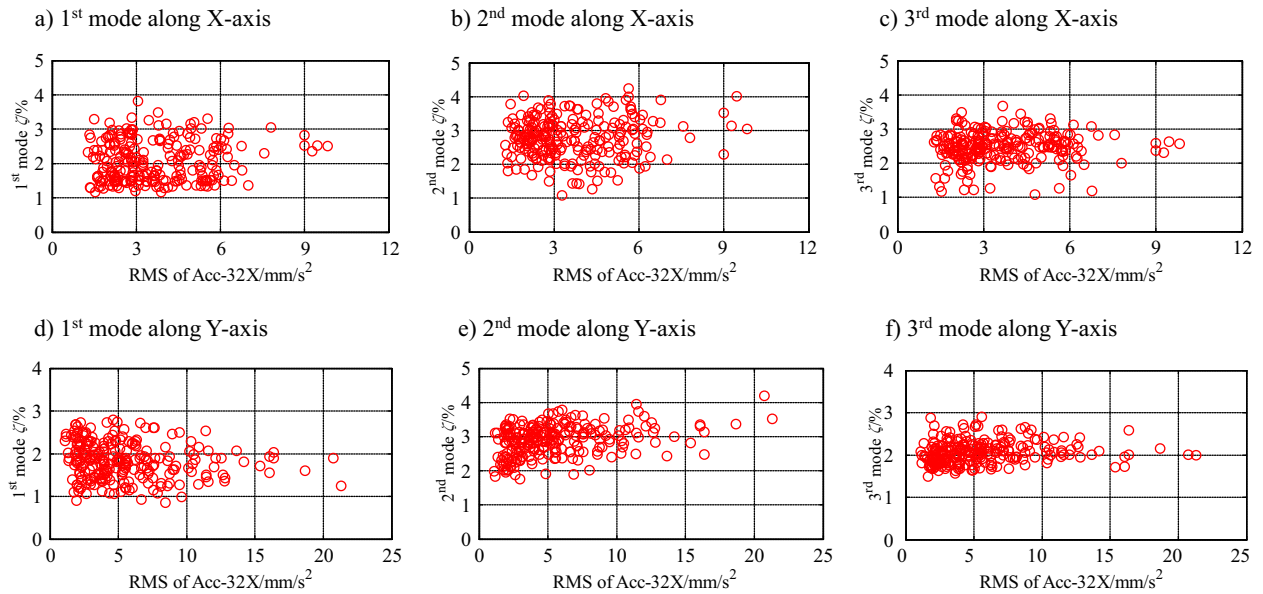
Figure 18. The relationship between modal damping ratios and RMS of Acc at the top floor

along X-axis are within 0.8–4.5%, and within 0.8–4.0% along Y-axis. The modal damping ratio identified by RDT and Morlet-type time-frequency wavelet transform methods has different deviation, which is not only related to the recorded signal quality, but also directly related to the factorization and the selection of the system orders by processing technology. However, the current identifications of modal damping ratios are based on the approximate estimation, and there is no widely accepted technology for modal damping ratio identifications especially when the recorded signals with short duration are subjected to the narrow-band non-stationary excitation. Therefore, this paper mainly focuses on the rule judgment of the amplitude-dependent modal damping ratio. Figure 17 shows 10-min variations of the amplitude-dependent modal ratio identified by RDT and Morlet-type time-frequency wavelet transform methods, and proves that the rules of recognition results identified by two methods are basically the same. The measured modal ratios of high-rise buildings under typhoon excitation are larger than those under static wind condition. This phenomenon shows that the measured modal ratios along X and Y axes are closely related to the acceleration amplitude of the measured high-rise building. When the RMS of translational acceleration is less than a critical amplitude of 5 mm/s^2 at the top floor, the modal ratios along X and Y axes of the measured high-rise building increase sharply. When the RMS of translational acceleration is greater than 5 mm/s^2. The damping ratio increases gradually at the initial stage of vibration, mainly because the structural damping ratio increases with the increasing vibration amplitude in the elastic stage, and the vibration amplitude of high-rise building increases gradually in the higher wind speed and reach a critical amplitude proposed by Aquinon and Tamura, and the first three modal damping ratios reach the maximum values. When RMS of accelerations are more significant than the critical amplitude, the damping ratio

gradually stabilizes, but it won't exceed the damping ratio under the critical amplitude.

Considering the non-stationary response of typhoon, this paper analyzes the measured damping ratio and acceleration amplitude by Morlet wavelet, and the results shown in Figure 18. The identified modal damping ratio is scattered when the basic time interval is 1 minute, and the identified results are within 1–5%, while the modal damping ratio is stably identified by the 10-min time domain method, which indicates that the selection of basic time interval has direct and significant influence on the identification of modal parameters.

Conclusions

By analyzing the measured data of Typhoons Sarika, Mujigae, Kalmaegi, and Rammasun, the wind field characteristics atop the building and axial acceleration responses at different floors along both the X and Y axes were obtained. By use of the Morlet wavelet to explore the modal characteristics, the following main conclusions are drawn as follows:

(1) The aspect ratio and width-thickness ratio of the in situ high-rise building are 6.71 and 1.47, respectively. The maximums of measured mean wind speeds atop the building are 48.0 m/s, 22.3 m/s, 20.4 m/s, and 20.0 m/s respectively; and their corresponding peak values of maximum acceleration are 0.359 m/s^2, 0.084 m/s^2, 0.044 m/s^2, and 0.079 m/s^2 under the influences of Typhoons Rammasun, Kalmaegi, Mujigae, and Sarika accordingly.

(2) The measured modal frequencies along X and Y axes are closely related to the acceleration amplitude of the measured high-rise building. When the RMS of accelerations is less than 5 mm/s^2 at the top floor, the modal frequencies along X and Y axes of the high-rise building decrease sharply.

When the RMS of accelerations is greater than 5 mm/s^2, the frequency reduction rate reduces after reaching a critical amplitude.

(3) The results show that the variation trend of modal frequency with acceleration amplitude identified by the Morlet wavelet is the same as that recognized by time-domain method, while it is scattered with the interval bar (min-average-max) due to the non-stationary response of Typhoon. Meanwhile, the larger the amplitude of acceleration response of high-rise buildings under strong wind, the greater the time-varying fluctuation of modal parameters identified by wavelet transform, and the bigger the difference between the interval bar (min-average-max).

(4) The identified modal damping ratio is scattered and the identified results are within 0.5–4.5% by Morlet wavelet, while the modal damping ratio is stably identified by the 10 min time-domain method, which indicates that the selection of basic time interval has direct and significant influence on the identification of modal parameters. It is difficult in drawing a trend or meaningful conclusion directly from Morlet wavelet method with respect to the response amplitude, thus the methods with 10 min are more reliable to give a better view of the results.

Acknowledgements

References

Boggs, D. W. (1992). Validation of the aerodynamic model method. *Journal of Wind Engineering and Industrial Aerodynamics*, *42*(1–3), 1011–1022. https://doi.org/10.1016/0167-6105(92)90107-L

Chang, F. K. (1973). Human response to motions in tall buildings. *Journal of the Structural Division*, *99*, 1259–1272. https://doi.org/10.1061/JSDEAG.0003785

Chen, X., & Huang, G. (2009). Evaluation of peak resultant response for wind-excited tall buildings. *Engineering Structures*, *31*(4), 858–868. https://doi.org/10.1016/j.engstruct.2008.11.021

Chen, X. (2013). Estimation of stochastic crosswind response of wind-excited tall buildings with nonlinear aerodynamic damping. *Engineering Structures*, *56*(6), 766–778. https://doi.org/10.1016/j.engstruct.2013.05.044

Cooper, K. R., Nakayama, M., Sasaki, Y., Fediw, A. A., Resende-Ide, S., & Zan, S. J. (1997). Unsteady aerodynamic force measurements on a super-tall building with a tapered cross section. *Journal of Wind Engineering and Industrial Aerodynamics*, *72*(1), 199–212. https://doi.org/10.1016/S0167-6105(97)00258-4

Gabbai, R. D., & Simiu, E. (2010). Aerodynamic damping in the along-wind response of tall buildings. *Journal of Structural Engineering*, *136*(1), 117–119. https://doi.org/10.1061/(ASCE)0733-9445(2010)136:1(117)

Hu, J. X., Li, Li, Z. N., & Zhao, Z. F. (2022). Full-scale measurements of translational and torsional dynamics characteristics of a high-rise building during typhoon Sarika. *Materials*, *15*(2), 493. https://doi.org/10.3390/ma15020493

Isyumov, N. (1999). Overview of wind action on tall buildings and structure. In *Proceedings of 10th International Conference on Wind Engineering* (pp. 15–28), Copenhagen, Denmark.

Jeary, A. P. (1992). Establishing non-linear damping characteristics of structures from non-stationary response time histories. *Structural Engineer*, *70*(4), 61–66.

Kareem, A. (1982a). Acrosswind response of buildings. *Journal of Structural Engineering*, *108*(4), 869–887. https://doi.org/10.1061/(ASCE)0733-9445(1984)110:10(2553)

Kareem, A. (1982b). Fluctuating wind loads on buildings. *Journal of the Engineering Mechanics Division*, *108*(6), 1086–1102. https://doi.org/10.1061/JMCEA3.0002892

Kareem, A. (1978). *Wind excited motion of buildings* [thesis for the degree of doctor of philosophy]. Colorado State University at Fort Collin, Colorado, USA.

Kareem, A., & Gurley, K. (1996). Damping in structures: its evaluation and treatment of uncertainty. *Journal of Wind Engineering and Industrial Aerodynamics*, *59*(2–3), 131–157. https://doi.org/10.1016/0167-6105(96)00004-9

Kawai, H. (1992). Vortex induced vibration of tall building. *Journal of Wind Engineering and Industrial Aerodynamics*, *41*(1), 117–128. https://doi.org/10.1016/0167-6105(92)90399-U

Kwok, K. C. S. (1982). Cross-wind response of tall buildings. *Engineering Structures*, *4*(4), 256–262. https://doi.org/10.1016/0141-0296(82)90031-1

Kwok, K. C. S., & Melbourne, W. H. (1981). Wind-induced lock-in excitation of tall structures. *Journal of the Structural Division*, *107*(1), 57–72. https://doi.org/10.1061/JSDEAG.0005637

Le, T. H., & Caracoglia, L. (2015). Wavelet-Galerkin analysis to study the coupled dynamic response of a tall building against transient wind loads. *Engineering Structures*, *100*, 763–778. https://doi.org/ 10.1016/j.engstruct.2015.03.060

Li, Z. N., Hu, J. X., Zhao, Z. F., & Wang, C. Q. (2018). Dynamic system identification of a high-rise building during Typhoon Kalmaegi. *Journal of Wind Engineering and Industrial Aerodynamics*, *181*, 141–160. https://doi.org/10.1016/j.jweia.2018.07.023

Marukawa, H., Kato, N., Fujii, K., & Tamura, Y. (1996). Experimental evaluation of aerodynamic damping of tall buildings. *Journal of Wind Engineering and Industrial Aerodynamics*, *59*(2), 177–190. https://doi.org/10.1016/0167-6105(96)00006-2

Piccardo, G., & Solari, G. (1996). A refined model for calculating 3-D equivalent static wind forces on structures. *Journal of Wind Engineering and Industrial Aerodynamics*, *65*(1–3), 21–30. https://doi.org/10.1016/S0167-6105(97)00019-6

Tamura, Y., Shimada, K., Sasaki, A., Kohsaka, R., & Fujii, K. (1995). Variation of structural damping ratios and natural frequencies of tall buildings during strong winds. In *Proceedings of 9th International Conference on Wind Engineering* (pp. 1396–1407), New Delhi, India.

Tanaka, H., Tamura, Y., Ohtake, K., Nakai, M., & Yong, C. K. (2012). Experimental investigation of aerodynamic forces and wind pressures acting on tall buildings with various unconventional configurations. *Journal of Wind Engineering and Industrial Aerodynamics*, *107–108*, 179–191. https://doi.org/10.1016/j.jweia.2012.04.014

The Ministry of Housing and Urban-Rural Development. (2012). *Chinese national loading specification for building structures* (GB 5009-2012). China.

Thepmongkorn, S., & Kwok, K. C. S. (2002). Wind-induced responses of tall buildings experiencing complex motion. *Journal of Wind Engineering and Industrial Aerodynamics*, *90*(4–5), 515–526. https://doi.org/10.1016/S0167-6105(01)00214-8

Thepmongkorn, S., Wood, G. S., & Kwok, K. C. S. (2002). Interference effects on wind-induced coupled motion of a tall building. *Journal of Wind Engineering and Industrial Aerodynamics*, *90*(12–15), 1807–1815.
https://doi.org/10.1016/S0167-6105(02)00289-1

Venanzi, I., Salciarini, D., & Tamagnini. C. (2014). The effect of soil–foundation–structure interaction on the wind-induced response of tall buildings. *Engineering Structures*, *79*(4), 117–130.
https://doi.org/10.1016/j.engstruct.2014.08.002

Vickery, B. J., & Stekley, A. (1993). Aerodynamic damping and vortex excitation on an oscillating prism in turbulent shear flow. *Journal of Wind Engineering and Industrial Aerodynamics*, *49*(1–3), 121–140.
https://doi.org/10.1016/0167-6105(93)90009-D

Yong, C. K., Kanda, J., & Tamura, Y. (2011). Wind-induced coupled motion of tall buildings with varying square plan with height. *Journal of Wind Engineering and Industrial Aerodynamics*, *99*(5), 638–650.
https://doi.org/10.1016/j.jweia.2011.03.004